

Geophysical Research Letters

RESEARCH LETTER

10.1029/2021GL093769

Key Points:

- The leading Tropical Atlantic climate modes shape the spatio-temporal variability of the Cold Tongue interannual surface Chlorophyll-a
- The Atlantic Zonal Mode explains the interannual Chlorophyll-a variability in the eastern part of the Cold Tongue with a peak in summer
- The North Tropical Atlantic Mode influences the interannual Chlorophyll-a variability in the western Cold Tongue, from spring to winter

Supporting Information:

Supporting Information may be found in the online version of this article.

Correspondence to:

F. Chenillat,
fanny.chenillat@ird.fr







Citation:

Chenillat, F., Illig, S., Jouanno, J., Awo, F. M., Alory, G., & Brehmer, P. (2021). How do climate modes shape the chlorophyll-a interannual variability in the tropical Atlantic? *Geophysical Research Letters*, 48, e2021GL093769. <https://doi.org/10.1029/2021GL093769>

Received 7 APR 2021

Accepted 28 MAY 2021

How do Climate Modes Shape the Chlorophyll-a Interannual Variability in the Tropical Atlantic?

F. Chenillat^{1,2} , S. Illig^{1,3} , J. Jouanno¹ , F. M. Awo^{3,4,5} , G. Alory¹ , and P. Brehmer^{2,6} 

¹LEGOS, CNES/CNRS/IRD/UPS, Toulouse, France, ²IRD, Univ Brest, CNRS, IFREMER, LEMAR, IRD DR Ouest, Plouzané, France, ³Department of Oceanography, MARIS Institute, University of Cape Town, Cape Town, South Africa, ⁴Department of Oceanography, Nansen-Tutu Centre for Marine Environmental Research, University of Cape Town, Cape Town, South Africa, ⁵ICMPA, Université d'Abomey Calavi, Cotonou, Benin, ⁶IRD, Univ Brest, CNRS, IFREMER, LEMAR, CSRP, Dakar, Senegal

Abstract Chlorophyll-a concentration (Chl-a) observed by satellite shows a marked seasonal and interannual variability in the Tropical Atlantic. This study analyzes how the remotely sensed surface Chl-a responds to the leading boreal summer climate modes affecting the interannual Tropical Atlantic variability over 1998–2018, corresponding to a positive Atlantic Multidecadal Oscillation phase. We show that the Atlantic Zonal Mode (AZM) and the North Tropical Atlantic Mode (NTAM) significantly drive the interannual surface Chl-a variability in the equatorial Atlantic, with different timings and contrasted zonal modulation of the Cold Tongue. The AZM involves remotely forced wave propagations favoring upwelling in the east and Chl-a modulation in the core of the Cold Tongue. Instead, the impact of the NTAM is mainly in the west, in response to locally forced pumping that modulates the western extension of the Cold Tongue. Such conditions can affect the marine food web, inducing significant variations for ecosystem functioning and fisheries.

Plain Language Summary The Tropical Atlantic Ocean is characterized by strong year-to-year surface temperature fluctuations which can be classified into basin-scale climate modes. In this study, we examine to which extent these modes of variability have a signature on the surface Chlorophyll-a concentration, a proxy of the biological activity at sea. Using two decades (1998–2018) of ocean-color satellite observations, we show that the interannual surface Chlorophyll-a modulation in boreal summer is impacted by these climate modes mainly along the equator. They drive contrasted Chlorophyll-a fluctuations in time and space. The first climate mode, the Atlantic Zonal Mode, involves distant mechanisms that propagate along the equator favoring biological activity in the eastern equatorial basin. Conversely, the second mode, the North Tropical Atlantic Mode, involves local mechanisms in the west of the equatorial band where it favors biological activity. Such conditions can affect the marine food web, inducing significant variations for the fisheries.

1. Introduction

The tropical Atlantic is characterized by a low-frequency variability of coupled ocean-atmosphere processes leading to extreme events with critical societal impacts (high rainfall, drought, hurricane; Foltz et al., 2019). These fluctuations, which mainly concern the Sea Surface Temperature (SST), occur at different time-scales from year-to-year variability to the Atlantic Multidecadal Oscillation (AMO, Kerr, 2000; Knight et al. 2006). The interannual variability is governed by two leading climate modes, namely the Atlantic Zonal Mode (AZM) and the North Tropical Atlantic Mode (NTAM) (Foltz & McPhaden, 2010; Xie & Carton, 2004). The AZM, also known as the Atlantic Niño or the Atlantic Equatorial Mode, is associated in its cold phase with anomalous cooling of boreal summer SST confined to the eastern equatorial basin, and conversely during its warm phase (Figure S1a; Kushnir et al., 2006; Lübbecke et al., 2018). In contrast, the NTAM, also known as the Atlantic Meridional Mode or Dipole mode, is characterized by an interhemispheric gradient of SST Anomalies (SSTA), with anomalous cold conditions in the north tropical Atlantic region and weak positive SSTA south of the equator during its cold phase, and conversely during its warm phase (Figure S1b; Chiang & Vimont, 2004). The NTAM usually peaks in boreal spring (Kushnir et al., 2006) and, notably, still has a signature in boreal summer (Amaya et al., 2017; Richter et al., 2013). Both modes are associated with changes in the ITCZ position, shifting equatorward (northward) in NTAM (AZM) cold phase, and conversely for

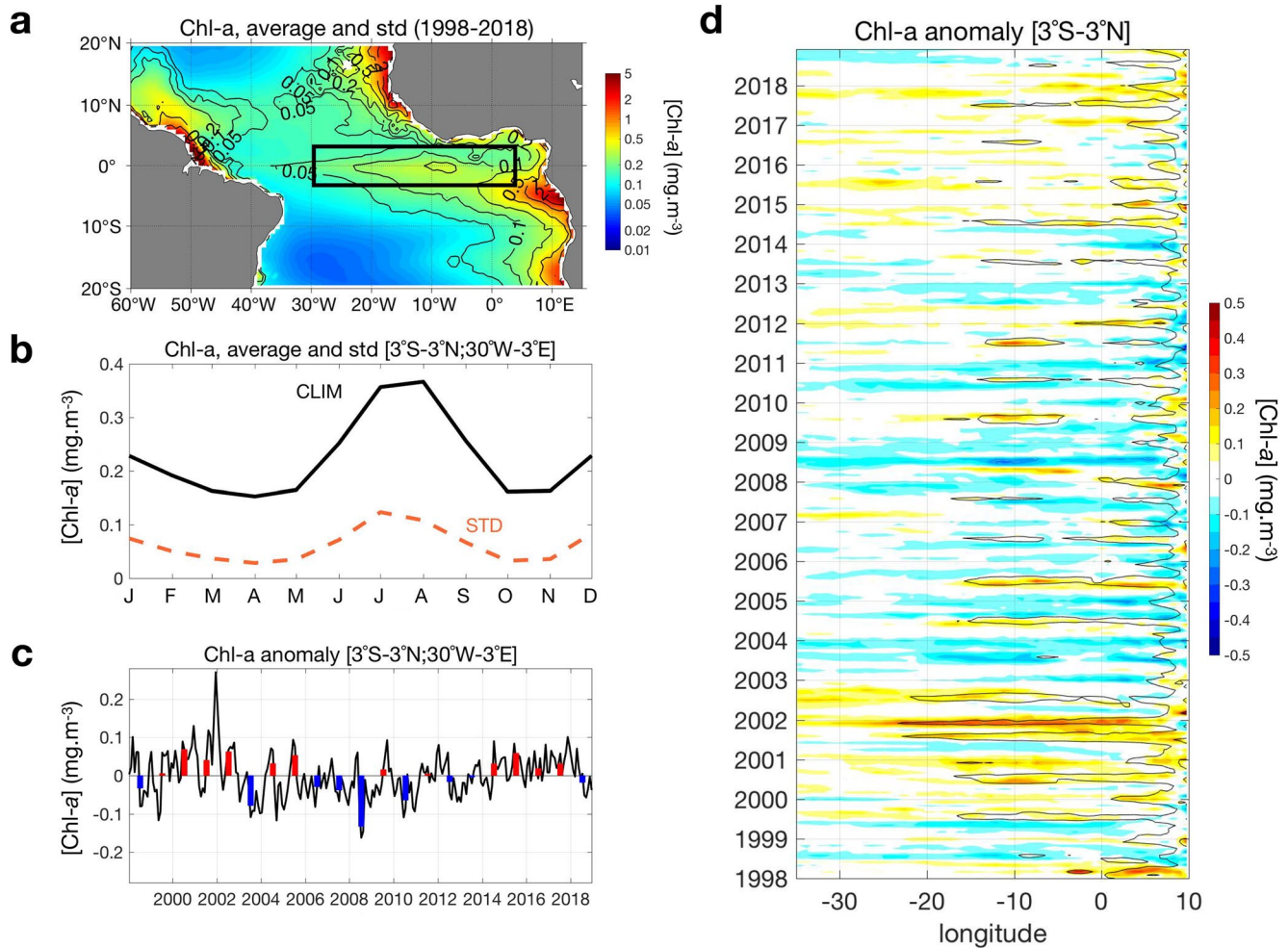


Figure 1. Temporal and spatial variability of surface chlorophyll-*a* concentration (Chl-*a*, $\text{mg}\cdot\text{m}^{-3}$) from satellite observations over 1998–2018. (a) Mean (color shading) and interannual standard deviation (black contours). (b) Climatological monthly mean (black line) and interannual monthly standard deviation (STD, orange dashed line) averaged over the Cold Tongue area (3°S – 3°N ; 30°W – 3°E), delineated by the black box in panel (a). (c) Monthly (black line) and boreal summer (June–July–August average, red/blue bars) interannual anomalies in the Cold Tongue. (d) Longitude–time Hovmöller diagram of the equatorial interannual anomalies averaged within (3°S – 3°N).

the warm phase (see Foltz et al., 2020 and references within). The imprint of these two interannual modes is directly modulated by the multidecadal variability, namely the AMO as shown in Martín-Rey et al. (2018). In particular, Vallès-Casanova et al. (2020) investigated the diversity of the Atlantic Niños and showed significant variations of the onset and duration of the SSTA they attributed to preconditioning driven by external forcing such as NTAM or Pacific El Niño.

This interannual variability of the tropical Atlantic is likely to impact the marine ecosystem. SST variability can indeed reflect the modulation of nutrient inputs through the thermocline depth displacements and result in the variability of chlorophyll-*a* concentration (Chl-*a*) and marine ecosystems. Actually, in such a region where there is no light-limitation at the surface, the primary production is predominantly driven by the nutrient availability in response to physical drivers (Longhurst, 1993; Longhurst, 2007). To our knowledge, the most extensive investigation of seasonal and interannual variability of Chl-*a* in the tropical Atlantic was carried out by Grodsky et al. (2008), using a 10-year-long time-series of sea surface Chl-*a*. Using an updated 21-year-long time-series of remote-sensed surface Chl-*a* (see Material & Methods), we confirm their results (Figures 1 and 1b): the richest surface waters are located along the coasts due to coastal upwelling and river discharges and also in the equatorial Atlantic Cold Tongue region where the equatorial upwelling prevails seasonal and interannual equatorial Chl-*a* variability peaks at (10°W , 0°N), spreading zonally from

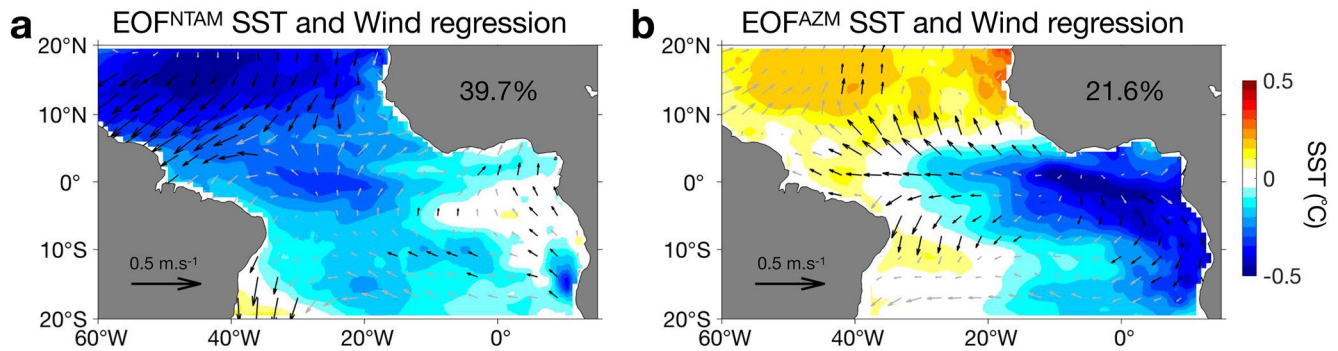


Figure 2. Maps of the two leading Empirical Orthogonal Function (EOF) of boreal summer “June-July-August” (JJA) interannual Sea Surface Temperature (SST) variability (color shading, °C) in the tropical Atlantic ([20°S–20°N, 60°W–15°E]) over the 1998–2018 period. The percentages indicate the explained variance of each mode. JJA surface wind interannual anomalies (arrows, $\text{m}\cdot\text{s}^{-1}$) are regressed onto the respective standardized Principal Component (PC, shown in Figures 3e and 3f). Significant values (>95% confidence level) are shown with black vectors. NTAM: North Tropical Atlantic mode. AZM: Atlantic Zonal mode.

0°E to 30°W (Figure 1a). It is maximum in boreal summer ($0.35 \pm 0.1 \text{ mg}\cdot\text{m}^{-3}$, Figure 1b). Surface Chl-a anomalies in the Cold Tongue show marked interannual variability (Figure 1c). This is even more striking when looking at the zonal extension of Chl-a anomalies along the whole equatorial waveguide (Figure 1d). Interestingly, while on average surface Chl-a interannual variability peaks around 10°W, it can extend over the whole equatorial Atlantic and peak at 25°W (e.g., in 2002).

Grotsky et al. (2008) hypothesized that interannual variability of the sea surface Chl-a and SST in the eastern equatorial Atlantic is driven by the thermocline displacements, associated with the interannual fluctuations of the equatorial zonal wind. However, the broader effect on primary productivity is still unknown (Foltz et al., 2019). This leads us to question the sources of such temporal and spatial variability of the sea surface Chl-a on an interannual timescale in the entire equatorial Atlantic. We will focus our study on the boreal summer period when seasonal and interannual variability of Chl-a is maximum (Figure 1b). In this paper, using remote-sensed observations over the equatorial Atlantic region, we describe how interannual climate modes shape the Chl-a variability in time and space.

2. Materials and Methods

This study has been conducted using ocean-color satellite data over the 1998–2018 period in the Tropical Atlantic region from 20°S to 20°N. Ocean-color, provided by E.U. Copernicus Marine Service Information, is a proxy for open-sea Chl-a (Fournier et al., 2015). We analyzed cloud-free Chl-a monthly maps (L4 product, CMEMS, 2020a), based on the Copernicus-GlobColour processing chain. Concomitant monthly SST and near-surface atmospheric circulation described through zonal and meridional wind components come from the European Center for Medium-Range Weather Forecasts ERA-Interim reanalysis (Dee et al., 2011). Monthly remote-sensed Sea Surface Height (SSH), a good approximation for the thermocline displacements, is available since 1993 from Aviso Ssalto/Duacs (Pujol et al., 2016) and provided by CMEMS (2020b).

After removing the global warming linear trend, monthly interannual anomalies are estimated relative to the 1998–2018 climatology. Due to the relative shortness of the time-series, we do not filter out the lower-frequency signal (Awo et al., 2018; Lübbecke et al., 2018; Prigent et al., 2020). We focus on the boreal summer Chl-a variability and, we average the data over the June-July-August (JJA) season. Diagnostics consist primarily of Empirical Orthogonal Function (EOF) analyses and linear regressions. The EOF analysis allows decomposing the Tropical Atlantic SSTA variability into a set of independent spatial modes (the EOFs, Figure 2) associated with distinct temporal fluctuations—the Principal Components (PCs, Figures 3e and 3f). Classically, PCs are normalized such as their standard deviation (STD) is 1 and the EOF spatial pattern conveys the unit of the variable. To isolate the part of the Chl-a, wind, and SSH variability associated with each leading EOF mode, we linearly regress (using a least mean square method) the interannual time-series onto the standardized PCs (Figures 3a–3d). The goodness of the linear fit is systematically measured by the square of the correlation coefficient (r^2) between PCs and the independent time-series.

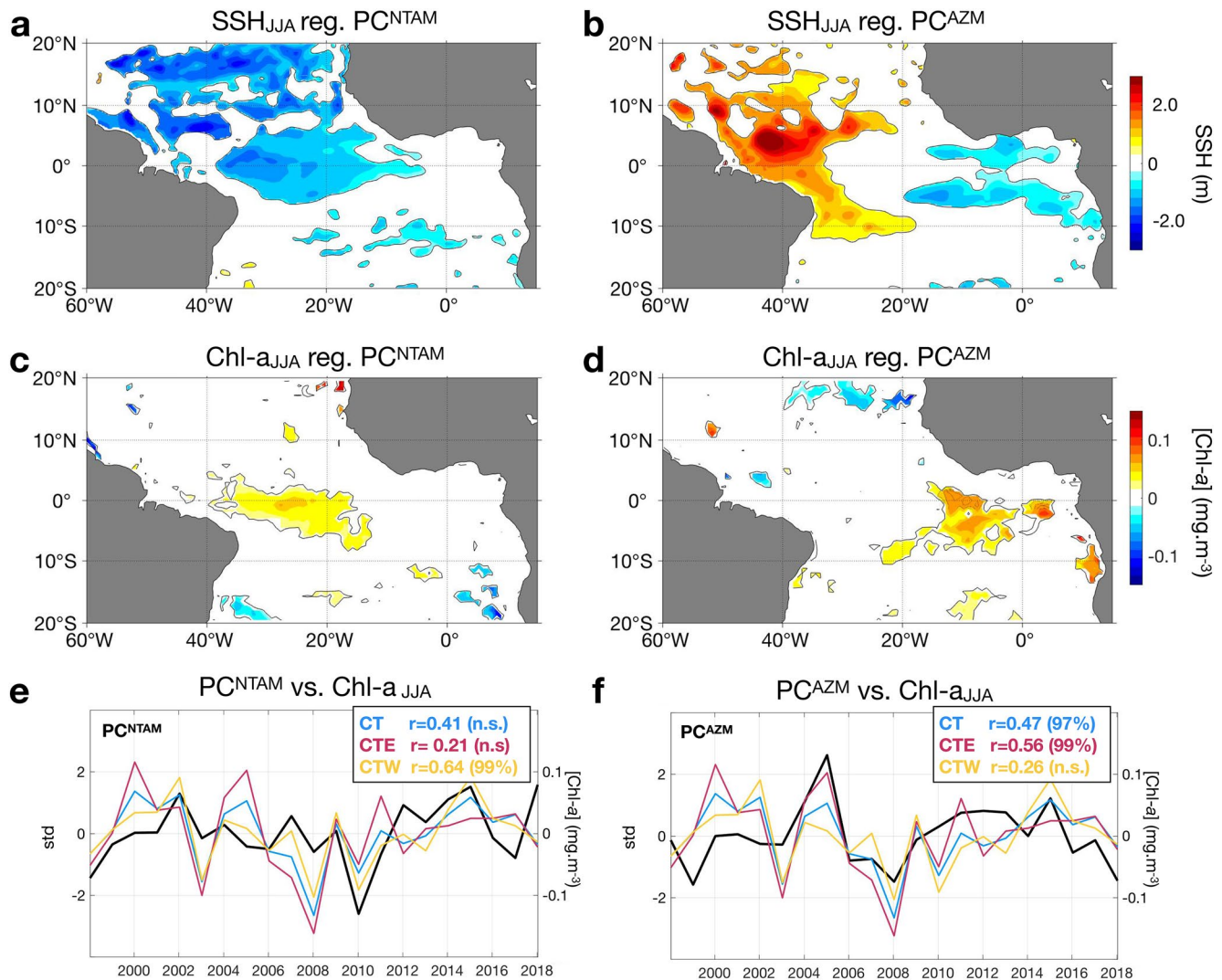


Figure 3. Spatio-temporal characteristics of the boreal summer (JJA) Sea Surface Height (SSH) and Chl-a associated with the NTAM and AZM interannual EOF modes of the Tropical Atlantic SST (presented in Figure 2). Regression maps of JJA SSH interannual anomalies (cm) onto the NTAM (a) and AZM (b) standardized Principal Components (PCs, shown in panels e–f (black lines)). Only significant values (>95% confidence level) are shaded. (c)–(d) Same as panels a–b for JJA Chl-a anomaly (mg.m⁻³). NTAM (e) and AZM (f) EOF PCs (black lines) are compared with boreal summer surface Chl-a interannual anomalies averaged in different portions of the Cold Tongue: entire Cold Tongue (CT, [3°S–3°N; 27°W–3°E], blue lines), eastern Cold Tongue (CTE, [3°S–3°N; 15°W–3°E], pink lines), and western Cold Tongue (CTW, [3°S–3°N; 27°W–15°W], orange lines). Correlation value (r) and associated significance level (%) quantify the goodness of the linear fit between PCs and Chl-a time-series. n.s.: not significant.

Throughout the study, the statistical significance of correlations is estimated based on Student's t-test at the 95% confidence level.

Because we aim at understanding Chl-a interannual variability, we preferentially focus on anomalous productive years corresponding to the occurrence of cold interannual events. We thus present the cold phase of the leading EOF modes of the Tropical Atlantic SST, inversely to the usual convention.

3. Climate Modes and Chl-a Variability

3.1. Tropical Atlantic Interannual Climate Modes Over a Positive AMO Phase

As expected, two leading modes of interannual climate variability emerge from the analysis of boreal summer tropical Atlantic SSTA (Figure 2). While these patterns stray from the classical climate modes (described in the introduction; Figure S1), they are consistent with Martín-Rey et al. (2018), who recently

diagnosed a modulation of the leading climate mode structures regarding the AMO phase. These results are coherent since EOFs analyses are performed over the last two decades (1998–2018) and that the AMO is in a positive phase since the 1990s (Wu et al., 2019).

The dominant mode explains 39.7% of the summer tropical Atlantic interannual variability. It is characterized by strong northern cold (warm) SSTA, accompanied by anomalous northeasterly (southwesterly) trades, contrasting with a near-zero positive (negative) SSTA south of the equator, confined to the eastern tropical Atlantic (Figure 2a). Such pattern resembles closely the NTAM pattern during positive AMO phases (Martín-Rey et al., 2018).

The second leading mode explains 21.6% of the summer tropical Atlantic interannual variability. It is characterized by strong cold (warm) SSTA in the eastern equatorial Atlantic extending southeastwards along the African coast in the Benguela upwelling system (Figure 2b) typical of an Atlantic Niña (Niño) event. Divergent (convergent) anomalous surface winds overlie the eastern equatorial Atlantic SSTA event (Illig et al., 2020), associated with a strengthening (relaxation) of the Trade winds in the western-central equatorial Atlantic and coastal poleward (equatorward) winds along the Benguela current system. A weak inter-hemispheric SSTA gradient is also depicted. This pattern is typical of the AZM during positive AMO phases (Martín-Rey et al., 2018).

Note that, in comparison with Martín-Rey et al. (2018), we find that the NTAM explains more variance than the AZM mode during a positive AMO phase. This can be attributed to the temporal restriction of our analysis (Lübbecke et al., 2018) (two decades against the juxtaposition of three periods accounting for 34 years in Martín-Rey et al. (2018)), consistently with a weakening of the SSTA variability in the eastern equatorial Atlantic (Prigent et al., 2020). A possible linear mix between the two climate modes (Hormann and Brandt, 2009; Servain et al., 1999) or the effect of climate change (Lübbecke et al., 2018) might also explain this difference.

3.2. NTAM and the Western Equatorial Chl-a Modulation

The interannual SSH Anomaly (SSHA) signature associated with the cold phase of the NTAM shows negative anomalies mostly in the northern Tropical Atlantic and in the western part of the equatorial band, from 40°W to 5°W with a peak at 40–30°W (Figure 3a). Considering the SSH as a proxy for the thermocline depth (Arnault et al., 1992), a cold-phase NTAM is mainly associated with a shoaling of the thermocline where negative SSHA are located (Martín-Rey et al., 2018). Such a thermocline rise is likely to be driven locally by a positive Ekman Pumping anomaly associated with the increased surface wind-stress curl (Figure S2). In the western equatorial sector, the shoaling of the thermocline is expected to enhance the equatorial upwelling and therefore increase the vertical nutrients flux into the euphotic layer and enhance the Chl-a in the surface layer. This mechanism is consistent with the Chl-a signature associated with the cold phase of the NTAM (Figure 3c). Positive Chl-a anomalies are indeed observed in the western part of the equatorial fringe collocated with the SSHA. They extend zonally from 40°W to 15°W with a peak near ~25°W. Such a close link between SSHA and Chl-a patterns suggests control of Chl-a by vertical processes, though vertical nutrient fluxes. There is, however, no significant modulation of the Chl-a anomalies in the northern Tropical Atlantic (5–15°N), despite despite significant negative SSHA. The apparent weak sensitivity of surface Chl-a in this region to climate modes would deserve further attention.

Consistently, the interannual modulation of NTAM (PC^{NTAM}) and the Chl-a averaged in the Cold Tongue region have a correlation of 0.41. Notably, this correlation substantially increases and becomes statistically significant when only the western part of the Cold Tongue (CTW) is considered ($r = 0.64$, >99%) (Figure 3e), with a regression coefficient of $-0.12 \text{ mg.m}^{-3}/^{\circ}\text{C}$. Conversely, the eastern Cold Tongue Chl-a variability is not correlated with PC^{NTAM} . Hence, the NTAM mode significantly explains the interannual boreal summer Chl-a variability in the western equatorial band with strong positive anomalies in 2002 and 2015 and negative anomalies in 2010 (also visible in Figures 1c and 1d). Interestingly, 2002 has been investigated by Hormann and Brandt (2009). They diagnosed 2002 as an abnormally warm year in the eastern part of the Cold Tongue contrasting with cold anomalies in the western part (west of 25°W), similarly to our cold-phase NTAM pattern (Figure 1a).

3.3. AZM and the Eastern Equatorial Chl-a Modulation

The cold phase of the AZM is associated with strong positive interannual SSHA in the western Tropical Atlantic, from 10°S to ~15–20°N, which contrasts with the negative SSHA in the Gulf of Guinea (east of 20°W) (Figure 3b). The latter are divided into two SSH depressions nearly symmetric about the Equator and centered ~4°–5° of latitude away from the Equator, typical of the signature of equatorial Rossby waves on the SSH. These upwelling waves are most likely associated with the reflection of eastward-propagating equatorial Kelvin waves forced earlier in the western equatorial basin by the zonal wind fluctuations associated with the AZM (Illig et al. 2004) (Figure 2b). Incidentally, part of the equatorial Kelvin wave energy could also have been transmitted along the African coast as coastally trapped waves, which would explain the remaining negative SSHA depicted off Angola (Bachelery et al., 2020). These interannual SSHA fluctuations reflect a substantial shoaling (deepening) of the thermocline in the eastern (western) tropical Atlantic. The rise of the thermocline would yield a positive nutrient advection into the sunlit layer and should explain the positive surface Chl-a anomalies in the eastern Cold Tongue and along the southern Angola Current (Figure 3d).

The interannual modulation of the AZM (PC^{AZM}) (Figure 3f) and the Chl-a averaged in the whole Cold Tongue region are significantly correlated ($r = 0.47$, >95%). This correlation slightly increases when only the eastern part of the Cold Tongue is considered ($r = 0.56$, >99%), with a regression coefficient of $-0.10 \text{ mg. m}^{-3}/^{\circ}\text{C}$, while the western Cold Tongue Chl-a variability is not correlated with PC^{AZM} . Therefore, we conclude that the AZM interannual climate mode significantly explains the interannual boreal summer Chl-a variability in the eastern equatorial band with a strong cold event in 2005 and a warm event in 2008 (also visible in Figures 1c and 1d). Hormann and Brandt (2009) have also analyzed the abnormally cold year of 2005. In contrast to 2002, during the boreal summer of 2005, the easterlies were stronger in the western basin, and the Equatorial Under Current was embedded in a shallower thermocline at 23°W. The thermocline was abnormally shallow in the whole eastern equatorial Atlantic (Marin et al., 2009) and was associated with a weak equatorial Kelvin wave activity. Vallès-Casanova et al. (2020) classified the year 2005 as a La Niña event, characterized by an early onset and persistent cold anomalies along the equator, peaking at 10°W in June.

3.4. Spatio-Temporal Modulation Under NTAM and AZM Influence

To diagnose the spatio-temporal modulation of the surface properties by the two leading climate modes, we linearly regress the 3-month running-mean of SST, surface wind, SSH, and Chl-a interannual anomalies onto the standardized PC^{NTAM} and PC^{AZM} (Figures 3e and 3f). Figure 4 presents a longitude-time Hovmöller diagram of the regression coefficients averaged in the equatorial band for the NTAM and AZM. A coherent longitude-time evolution of the key equatorial properties anomalies emerges for both modes and can be interpreted in the light of the climatological conditions (Figure S3).

For the NTAM, the cold phase is associated with a cold equatorial SSTA in the western basin, that progresses from the end of the boreal winter. It extends from the Brazilian coast to ~15°W and peaks in early boreal summer (MJJ) at ~30°W, concomitant with anomalous wind divergence (Figure 4a). Collocated with this cold event in the western equatorial Atlantic, Figure 4c discloses a strong and persistent negative SSHA and a positive Chl-a anomaly in boreal summer (MJJ and JJA). These physical and biogeochemical anomalies are concomitant and steady, which suggests that they are associated with local vertical processes consistent with the increased Ekman pumping diagnosed from the NTAM anomalous surface wind-stress curl (Figure S2). Concurrently, from boreal winter (JFM) to early summer (MJJ), relaxed easterlies are observed along the whole equatorial band. They drive downwelling equatorial Kelvin waves which reduce the equatorial upwelling in the eastern basin, leading to a strong zonal seesaw pattern in SSH, SST, and Chl-a anomalies. Note that Hormann and Brandt (2009), who studied a typical NTAM year (2002), also associated such a cold event with abnormally relaxed easterlies in the western basin. They emphasized a strong Equatorial Under Current core embedded in a shallow thermocline at 23°W which is consistent with the anomalous positive Ekman Pumping triggered by the surface wind pattern discussed earlier. Interestingly, during the following boreal fall, the cold anomaly slowly progresses eastwards east of 20°W, accompanied by a negative SSHA and a positive Chl-a anomaly. Also, the NTAM boreal summer western cold event is preceded by cold SSTA in the eastern basin in boreal winter (DJF), associated with negative SSHA and positive Chl-a anomalies.

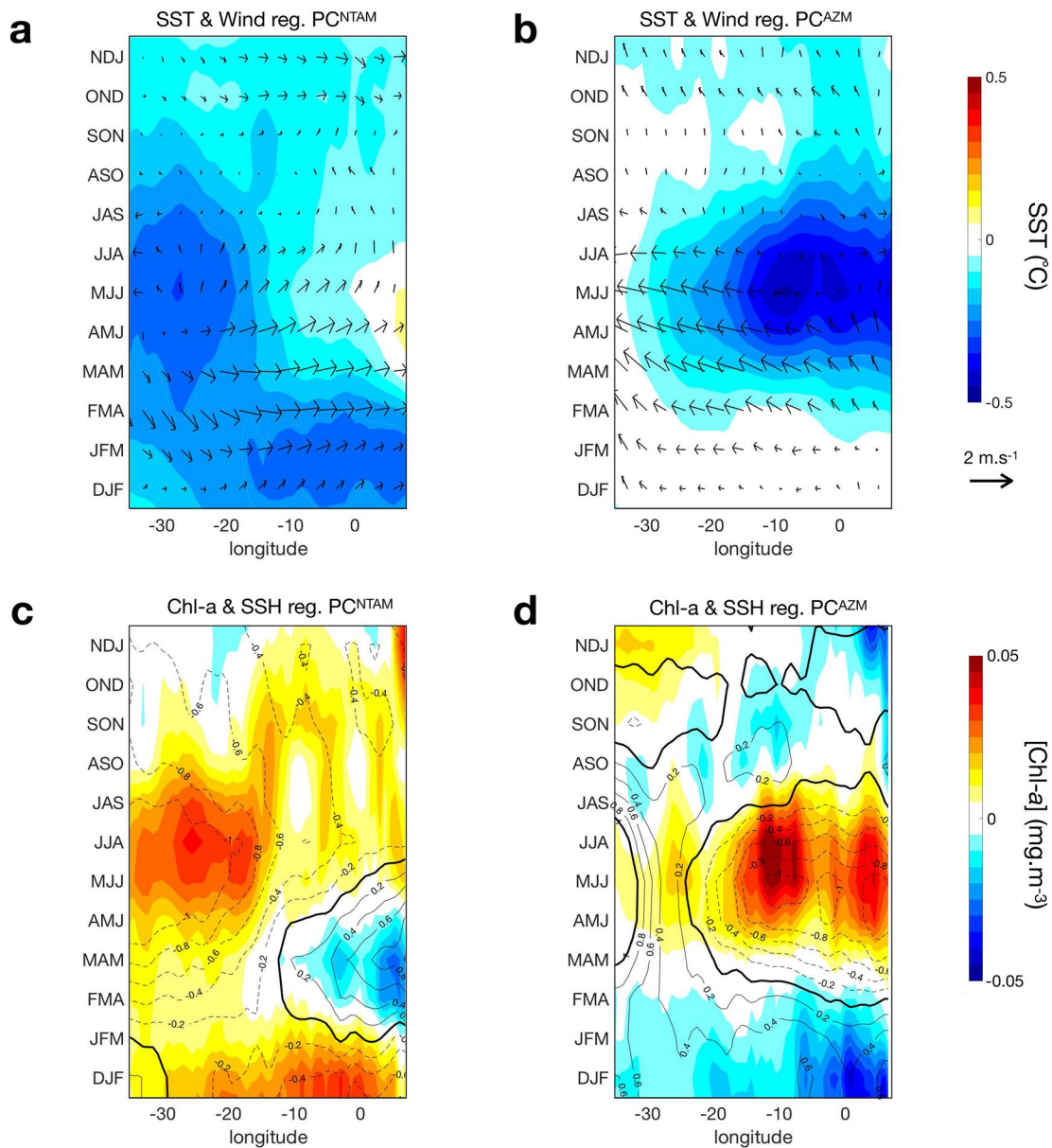


Figure 4. Phenology of equatorial surface properties associated with NTAM (left panels) and AZM (right panels) EOF modes of JJA interannual Tropical Atlantic SSTA. 3-month running-mean of SST, surface wind, SSH, and Chl-a interannual anomalies from preceding winter (DJF) to following winter (NDJ) are regressed onto the standardized PCs (shown in Figures 3e and 3f) and averaged within $[3^{\circ}\text{S}-3^{\circ}\text{N}]$. SSTA (color shading, $^{\circ}\text{C}$) and surface wind anomalies (arrows, $\text{m}\cdot\text{s}^{-1}$) associated with JJA NTAM and AZM are displayed on top panels. On bottom panels, same for Chl-a (color shading, $\text{mg}\cdot\text{m}^{-3}$) and SSH (contours, cm) interannual anomalies.

This pattern is typical of the boreal winter Atlantic Niño II from Okumura and Xie (2006), shown to act as preconditioning to the subsequent boreal spring NTAM. However, the wind forcing of this zonal mode does not seem to be captured by our methodology designed to study the spring/summer variability.

For the AZM, the cold phase is associated with a cold equatorial anomaly extending east of $\sim 20^{\circ}\text{W}$ to the African coast. The cold event spreads slowly westwards from late winter and is maximum in early boreal summer (MJJ) at $\sim 10^{\circ}\text{W}$ (Figure 4b, coherently with La Niña pattern from Vallès-Casanova et al., 2020). This eastern cold anomaly is driven by an intensification of easterly trades along the equator initiated in boreal winter (JFM) and persisting until the following summer (JJA) (Figure 4b). Concomitant to this cold SSTA, a strong negative SSHA and a positive Chl-a anomaly are depicted (Figure 4d). The latter can be attributed to

the enhanced upwelling of cold nutrient-rich deep water into the surface layer (Radenac et al., 2020), driven by remotely forced equatorial wave triggered by the reinforcement of easterly trades in the western-central basin. This analysis also reveals a localized moderate positive Chl-a MJJ peak at 25°W which seems to detach itself from the core eastern Chl-a anomaly and differs from the SSTA pattern. After the summer, an abrupt termination of the interannual event (Figures 4b and 4d) is associated with an eastward propagation of moderate positive SSHA and negative Chl-a anomalies that crosses the basin in ~2 months (from JAS to SON). The timing and characteristics of this propagation are consistent with a Kelvin wave triggered by the reflection of a downwelling Rossby wave forced upstream the relaxation of the easterlies. Notably, similar to the NTAM signature, an eastern negative Chl-a anomaly associated with a positive SSHA are observed at the beginning of the year. They may contribute to the modulation of eastern boreal winter Cold Tongue bloom (also visible in Figures 1b and 1d; Perez et al., 2005; Grodsky et al. 2008; Radenac et al. 2020). The study of the winter bloom is beyond the scope of this paper, but additional attention could be given to its interannual variability in future research projects.

4. Concluding Remarks

This study aims at describing how interannual climate modes shape the Tropical Atlantic Chl-a variability in time and space using a 21-year-long time-series remote-sensed observations over the equatorial Atlantic region. As expected, two leading modes of interannual climate variability emerge from our analysis of boreal summer (JJA) tropical Atlantic SSTA: namely the AZM and NTAM. Both NTAM and AZM spatial patterns do not strictly fit their canonical signature but are under the influence of a positive AMO phase (1998–2018) (Martín-Rey et al., 2018).

We show that AZM and NTAM significantly drive the interannual surface Chl-a variability in the equatorial Atlantic, with different timings and contrasted modulation in the Cold Tongue. The NTAM influences preferentially the interannual Chl-a variability in the western Cold Tongue, from boreal spring to fall (peaking in summer), while the AZM affects to a large extent, the interannual Chl-a variability in the eastern Cold Tongue, during boreal summer. Our results suggest that the significant surface wind anomalies in the western equatorial Atlantic associated with each climate mode have distinct effects on the ocean dynamics. The relaxation of easterlies in boreal winter associated with the cold phase of NTAM yields a shoaling of the western equatorial thermocline through Ekman pumping, while the AZM cold-phase intensification of easterlies in boreal spring triggers equatorial Kelvin wave propagation responsible for an anomalous shoaling of the thermocline in the eastern Cold Tongue region 1–2 months later. The locally and remotely forced vertical fluxes advect nutrients into the euphotic layer and increase the primary production in the western and eastern Cold Tongue region, respectively. This east/west contrast in the interannual Chl-a fluctuations is confirmed by an EOF analysis on the Chl-a restricted over the 3°S–3°N equatorial band (Figure S4). The first leading mode is associated with a strong positive anomaly along the equator (with peaks at 25, 18, and 10°W) with a temporal modulation significantly correlated with PC^{NTAM} ($r = 0.53$). The second leading mode highlights an east/west dipole of Chl-a anomalies (peaking at 10°W and 30°W, respectively) with a temporal modulation significantly correlated with PC^{AZM} ($r = 0.61$). Additionally, similar east/west partition of the equatorial Atlantic has already been documented (Longhurst, 2007; Longhurst et al. 2007; Perez et al. 2005), but simply based on the seasonality of biogeochemical properties, discriminating the variability in the Eastern Tropical Atlantic Province and the Western Tropical Atlantic Province, associated with a large boreal summer variability and a reduced boreal autumn peak, respectively.

This work provides new insights into the interannual variability of Chl-a, and its zonal signature, in this under-explored region. The role of such climate variability on Chl-a is likely to arise a myriad of biogeochemical implications. The challenge now is to understand how these climate modes impact the interannual spatio-temporal variability of the planktonic ecosystem, their consequences on the biological carbon pump and the higher trophic levels. In-depth analyses using a coupled physical-biogeochemical model are under investigation to diagnose biological-physical processes such as advective and diffusive nutrient fluxes and their potential impact on subsurface Chl-a and plankton ecosystem dynamics.

Data Availability Statement

The reanalysis data were downloaded from ECMWF (<http://www.ecmwf.int>).

Acknowledgments

This work is part of the TRIATLAS European project (South and Tropical Atlantic climate-based marine ecosystem prediction for sustainable management; H2020 grant agreement No 817578) which supported a post-doc fellowship funded by Institut de Recherche pour le Développement (IRD-France).

References

- Amaya, D. J., DeFlorio, M. J., Miller, A. J., & Xie, S.P. (2017). WES feedback and the Atlantic Meridional Mode: Observations and CMIP5 comparisons. *Climate Dynamics*, 49, 1665–1679. <https://doi.org/10.1007/s00382-016-3411-1>
- Arnault, S., Morlière, A., Merle, J., & Ménard, Y. (1992). Low-frequency variability of the tropical Atlantic surface topography: Altimetry and model comparison. *Journal of Geophysical Research*, 97(C9), 14259–14288. <https://doi.org/10.1029/92JC00818>
- Awo, F. M., Alory, G., Da-Allada, C. Y., Delcroix, T., Jouanno, J., Kestenare, E., & Baloitcha, E. (2018). Sea surface salinity signature of the tropical Atlantic interannual climatic modes. *Journal of Geophysical Research: Oceans*, 123, 7420–7437. <https://doi.org/10.1029/2018JC013837>
- Bachelery, M. L., Illig, S., & Rouault, M. (2020). Interannual coastal trapped waves in the Angola-Benguela upwelling system and Benguela Niño and Niña events. *Journal of Marine Systems*, 203(March 2020), 103262. <https://doi.org/10.1016/j.jmarsys.2019.103262>
- Chiang, J. C. H., & Vimont, D. J. (2004). Analogous Pacific and Atlantic meridional modes of tropical atmosphere-ocean variability. *Journal of Climate*, 17(21), 4143–4158. <https://doi.org/10.1175/jcli4953.1>
- CMEMS (2020). (E.U. Copernicus Marine Service Information). *Global ocean chlorophyll, pp and pft (copernicus-globcolour) from satellite observations: Monthly and daily interpolated (reprocessed from 1997)*, Accessed: 15 september 2020. <http://dx.doi.org/10.5194/os-15-819-2019>
- CMEMS (2020). (E.U. Copernicus Marine Service Information). *Global ocean gridded L4 sea surface heights and derived variables reprocessed (copernicus climate service)*, Accessed: 20 october 2020. Retrieved from <https://resources.marine.copernicus>
- Dee, D. P., Uppala, S. M., Simmons, A. J., Berrisford, P., Poli, P., Kobayashi, S., et al. (2011). The ERA-Interim reanalysis: Configuration and performance of the data assimilation system. *Quarterly Journal of the Royal Meteorological Society*, 137(656), 553–597. <https://doi.org/10.1002/qj.828>
- Foltz, G., Brand, P., Richter, I., Rodríguez-Fonseca, B., Hernandez, F., Dengler, M., et al. (2019). The tropical Atlantic observing system. *Frontiers in Marine Science*, 6, 206. <https://doi.org/10.3389/fmars.2019.00206>
- Foltz, G. R., & McPhaden, M. J. (2010). Interaction between the Atlantic meridional and Niño modes. *Geophysical Research Letters*, 37, L18604. <https://doi.org/10.1029/2010GL044001>
- Fournier, S., Chapron, B., Salisbury, J., Vandemark, D., & Reul, N. (2015). Comparison of spaceborne measurements of sea surface salinity and colored detrital matter in the Amazon plume. *Journal of Geophysical Research: Oceans*, 120(5), 3177–3192. <https://doi.org/10.1002/2014jc010109>
- Grodsky, S. A., Carton, J. A., & McClain, C. R. (2008). Variability of upwelling and chlorophyll in the equatorial Atlantic. *Geophysical Research Letters*, 35, L03610. <https://doi.org/10.1029/2007GL032466>
- Hormann, V., & Brandt, P. (2009). Upper equatorial Atlantic variability during 2002 and 2005 associated with equatorial Kelvin waves. *Journal of Geophysical Research*, 114, C03007. <https://doi.org/10.1029/2008JC005101>
- Illig, S., Bachelery, M. L., & Lübbecke, J. F. (2020). Why do benguela niños lead atlantic niños? *Journal of Geophysical Research: Oceans*, 125(9), e2019JC016003. <https://doi.org/10.1029/2019jc016003>
- Illig, S., Dewitte, B., Ayoub, N., du Penhoat, Y., Reverdin, G., de Mey, P., et al. (2004). Interannual long equatorial waves in the tropical Atlantic from a high resolution OGCM experiment in 1981–2000. *Journal of Geophysical Research: Oceans*, 109, C02022. <https://doi.org/10.1029/2003JC001771>
- Kerr, R. A. (2000). A North Atlantic climate pacemaker for the centuries. *Science*, 288, 1984–1986. <https://doi.org/10.1126/science.288.5473.1984>
- Knight, J. R., Folland, C. K., & Scaife, A. A. (2006). Climate impacts of the Atlantic multidecadal oscillation. *Geophysical Research Letters*, 33, L17706. <https://doi.org/10.1029/2006GL026242>
- Kushnir, Y., Robinson, W. A., Chang, P., & Robertson, A. W. (2006). The physical basis for predicting Atlantic sector seasonal-to-interannual climate variability. *Journal of Climate*, 19, 5949–5970. <https://doi.org/10.1175/jcli3943.1>
- Longhurst, A. R. (1993). Seasonal cooling and blooming in tropical oceans. *Deep-Sea Research*, 40, 2145–2165. [https://doi.org/10.1016/0967-0637\(93\)90095-k](https://doi.org/10.1016/0967-0637(93)90095-k)
- Longhurst, A. R. (2007). *Ecological geography of the sea*. Academic Press. <https://doi.org/10.1016/B978-0-12-455521-1.X5000-1>
- Lübbecke, J. F., Rodríguez-Fonseca, B., Richter, I., Martín-Rey, M. M., Losada, T., Polo, I., & Keenlyside, N. S. (2018). Equatorial Atlantic variability—Modes, mechanisms, and global teleconnections. *WIREs Climate Change*, 9(4), e527. <https://doi.org/10.1002/wcc.527>
- Marin, F., Caniaux, G., Giordani, H., Bourlès, B., Gouriou, Y., & Key, E. (2009). Why were sea surface temperatures so different in the Eastern equatorial Atlantic in June 2005 and 2006? *Journal of Physical Oceanography*, 39(6), 1416–1431. <https://doi.org/10.1175/2008JPO4030.1>
- Martín Rey, M., Polo, I., Rodríguez-Fonseca, B., Losada, T., & Lazar, A. (2018). Is there evidence of changes in tropical Atlantic variability modes under AMO phases in the observational record? *Journal of Climate*, 31(2), 515–536. <https://doi.org/10.1175/JCLI-D-16-0459.1>
- Okumura, Y., & Xie, S. (2006). Some overlooked features of tropical Atlantic climate leading to a new Niño-like phenomenon. *Journal of Climate*, 19(22), 5859–5874. <https://doi.org/10.1175/JCLI3928.1>
- Pérez, V., Fernández, E., Marañón, E., Serret, P., & García-Soto, C. (2005). Seasonal and interannual variability of chlorophyll a and primary production in the Equatorial Atlantic: In situ and remote sensing observations. *Journal of Plankton Research*, 27, 189–197.
- Prigent, A., Lübbecke, J. F., Bayr, T., Latif, M., & Wengel, C. (2020). Weakened SST variability in the tropical Atlantic Ocean since 2000. *Climate Dynamics*, 54, 2731–2744. <https://doi.org/10.1007/s00382-020-05138-0>
- Pujol, M.-L., Faugère, Y., Taburet, G., Dupuy, S., Pelloquin, C., Ablain, M., & Picot, N. (2016). DUACS DT2014: The new multi-mission altimeter data set reprocessed over 20 years. *Ocean Science*, 12, 1067–1090.
- Radenac, M.-H., Jouanno, J., Tchamabi, C. C., Awo, M., Bourlès, B., Arnault, S., & Aumont, O. (2020). Physical drivers of the nitrate seasonal variability in the Atlantic cold tongue. *Biogeosciences*, 17, 529–545. <https://doi.org/10.5194/bg-17-529-2020>
- Richter, I., Behera, S. K., Masumoto, Y., Taguchi, B., Sasaki, H., & Yamagata, T. (2013). Multiple causes of interannual sea surface temperature variability in the equatorial Atlantic Ocean. *Nature Geoscience*, 6(1), 43–47. <https://doi.org/10.1038/ngeo1660>
- Servain, J., Wainer, I., McCreary, J. P., & Dessier, A. (1999). Relationship between the equatorial and meridional modes of climatic variability in the Tropical Atlantic. *Geophysical Research Letters*, 26, 485–488. <https://doi.org/10.1029/1999gl900014>

- Vallès-Casanova, I., Lee, S. -K., Foltz, G. R., & Pelegrí, J. L. (2020). On the spatiotemporal diversity of Atlantic Niño and associated rainfall variability over West Africa and South America. *Geophysical Research Letters*, *47*, e2020GL087108. <https://doi.org/10.1029/2020GL087108>
- Wu, C.R., Lin, Y. F., Wang, Y.L., Keenlyside, N., & Yu, J. Y. (2019). An Atlantic-driven rapid circulation change in the North Pacific Ocean during the late 1990s. *Scientific Reports*, *9*, 14411. <https://doi.org/10.1038/s41598-019-51076-1>
- Xie, S.-P., & Carton, J. A. (2004). Tropical atlantic variability: Patterns, mechanisms, and impacts. In C. Wang, S. -P. Xie, & J. A. Carton (Eds.), *Earth's climate: The ocean-atmosphere interaction*, *Geophysical Monograph Series (121-142)*. American Geophysical Union.

Supplemental materials

**How do climate modes shape the
chlorophyll-a interannual variability
in the tropical Atlantic?**

Chenillat F., S. Illig, J. Jouanno, M. Awo, G. Allory and P. Brehemer

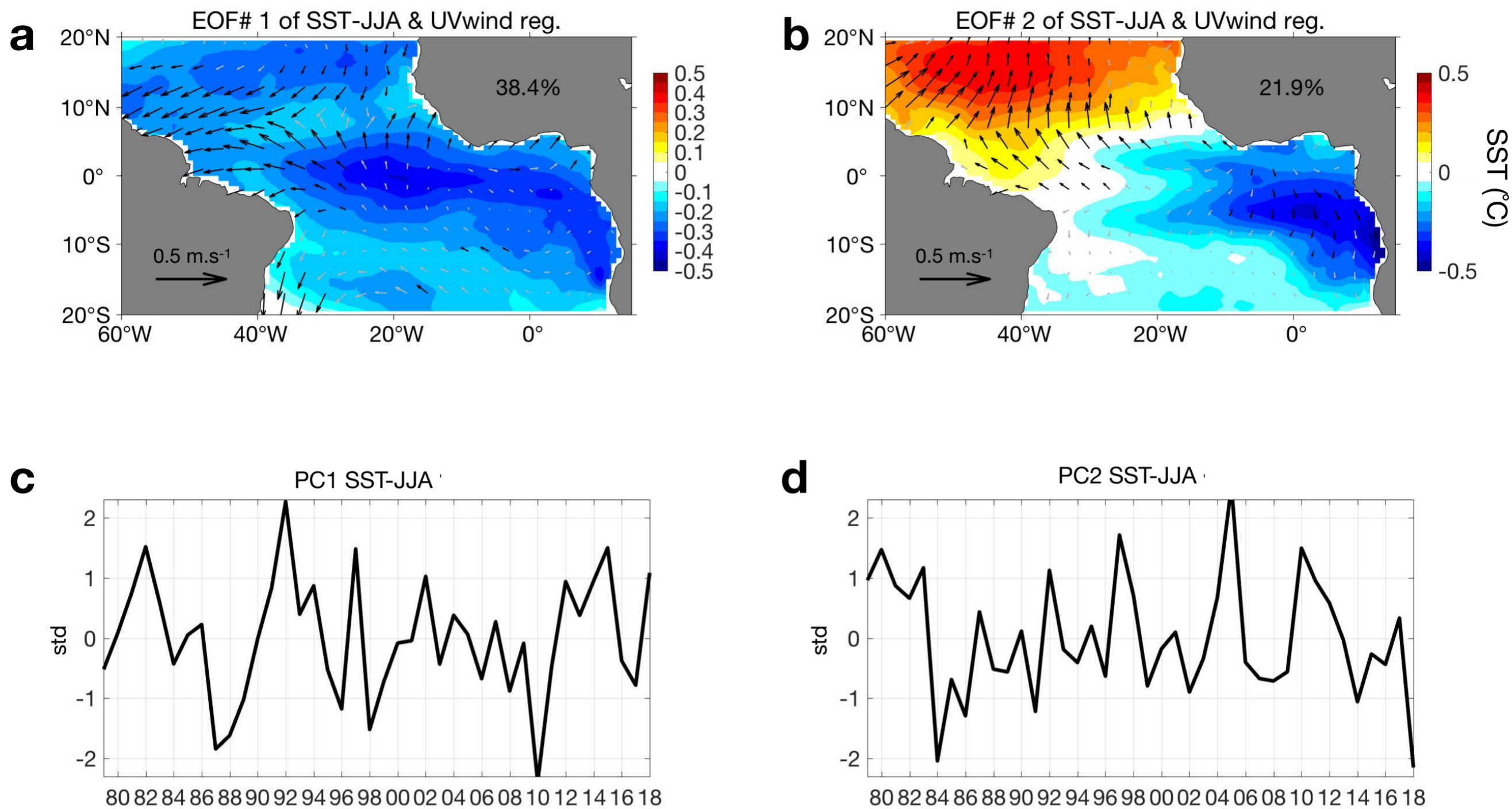


Figure S1: Maps of the two leading Empirical Orthogonal Function (EOF) of boreal summer (JJA) interannual SST variability (color shading, °C) in the tropical Atlantic ([20°S-20°N, 60°W-15°E]) over the 1979-2018 period. The percentages indicate the explained variance of each mode. JJA surface wind interannual anomalies (arrows, m.s⁻¹) are regressed on the respective normalized Principal Components (PC) shown in panel c and d. Significant values (> 95% confidence level) are shown with black vectors.

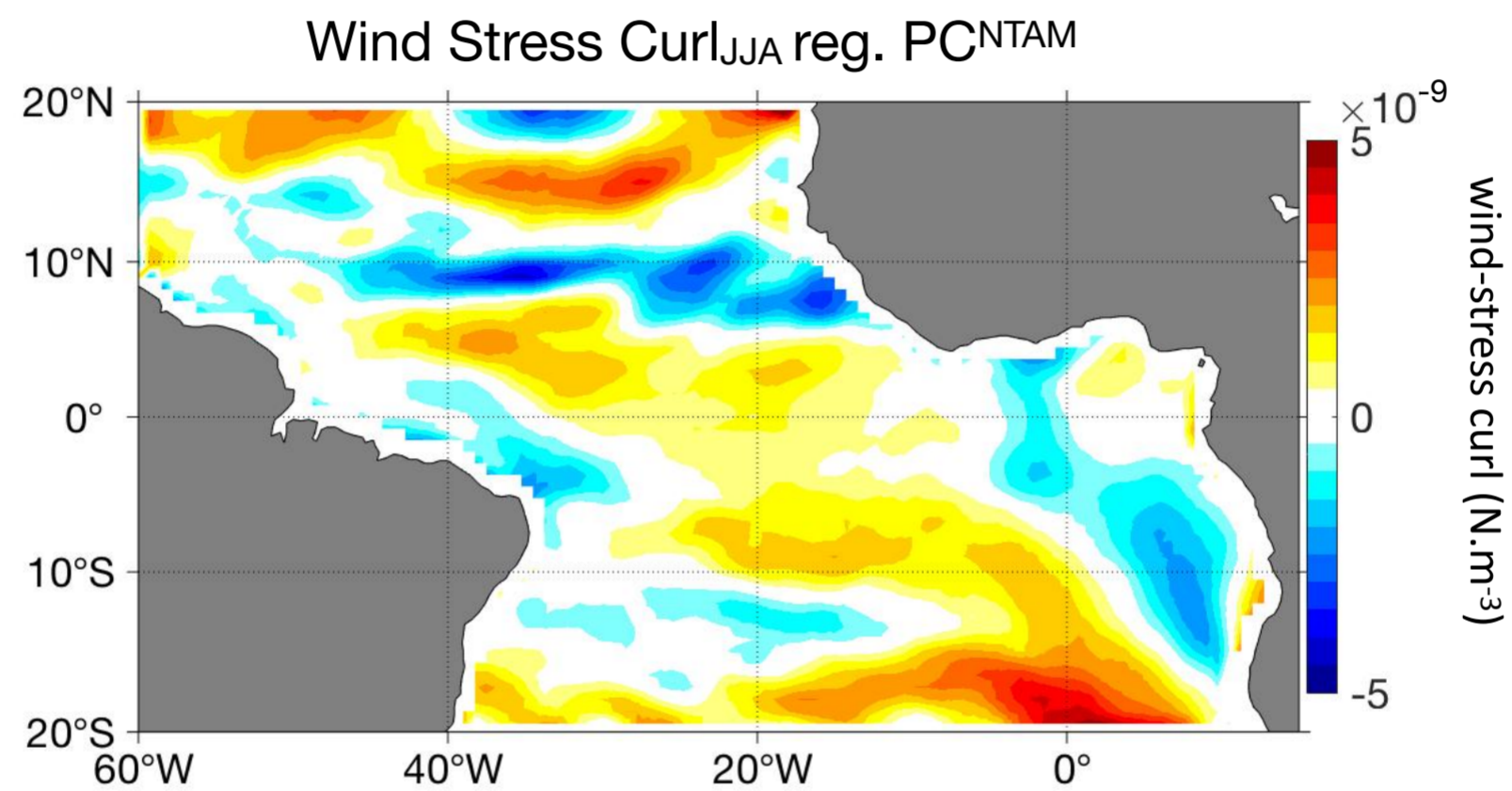


Figure S2: Surface wind-stress curl regressed on PC^{NTAM}. As for Fig.3a, we regressed maps of JJA surface wind-stress curl interannual anomalies (N.m⁻³) onto the standardized PC^{NTA} (shown in panels e, black line).

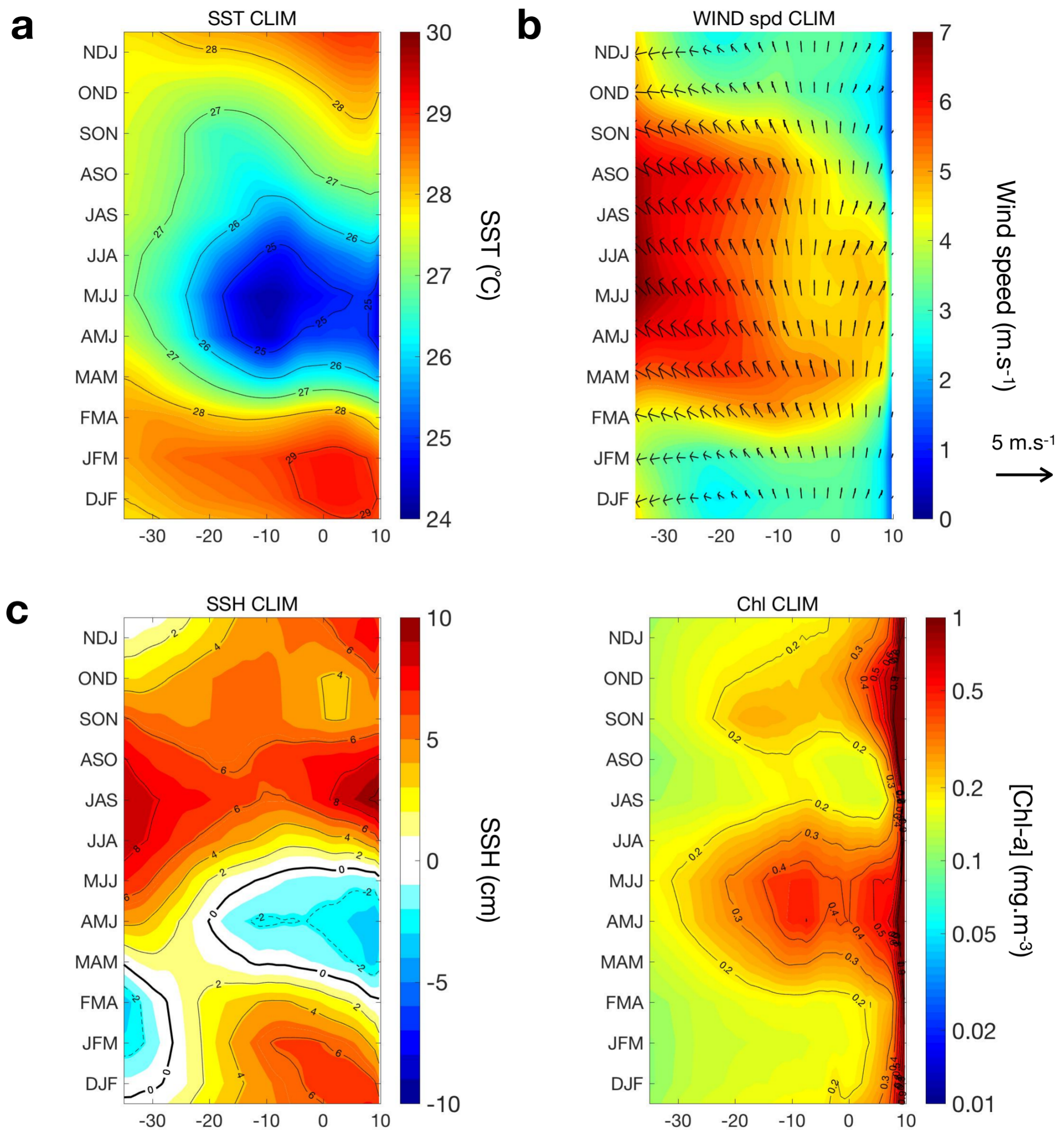


Figure S3: Phenology of climatology of equatorial (a) SST (°C), (b) surface wind speed (m.s⁻¹), (c) SSH (m), and (d) Chl-a (mg.m⁻³). All properties are averaged over the equatorial band [3°S-3°N]. Climatologies are computed for the entire available period for each variables, i.e., SST and winds are computed over 1979-2018, SSH over 1993-2018, and Chl-a over 1998-2018.

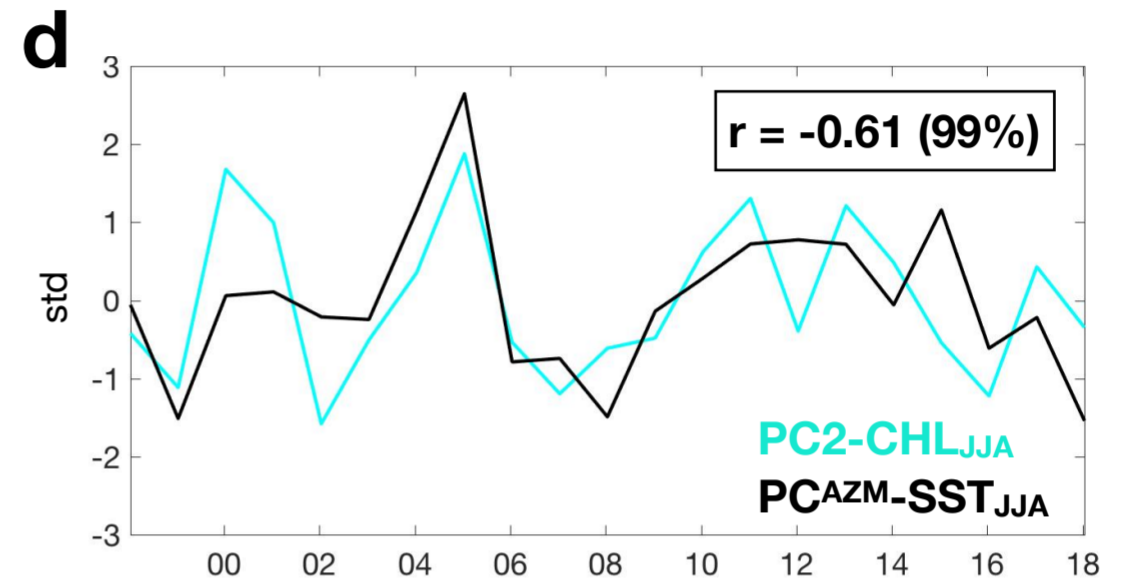
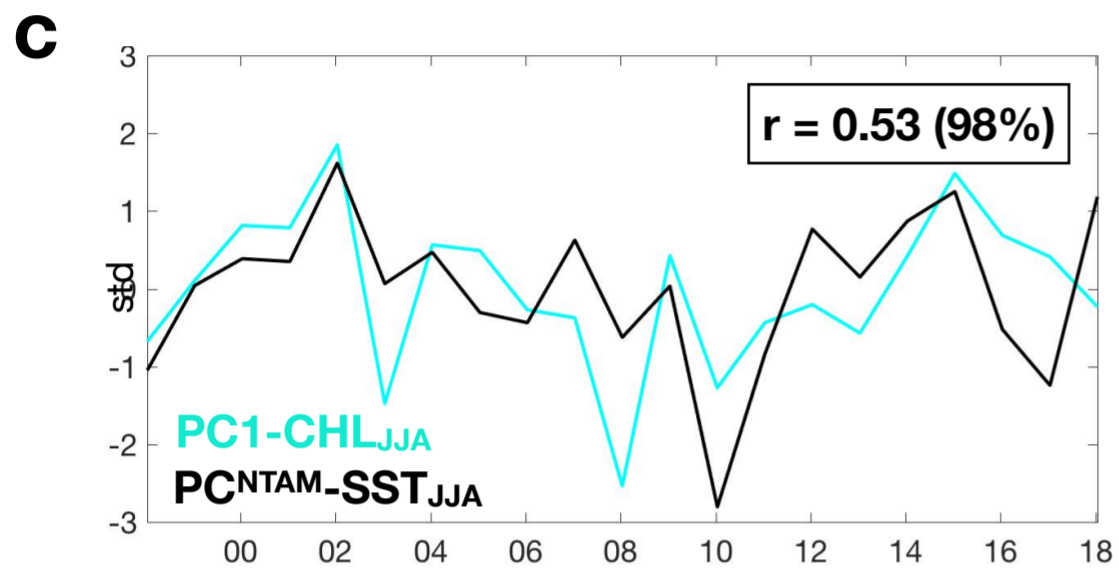
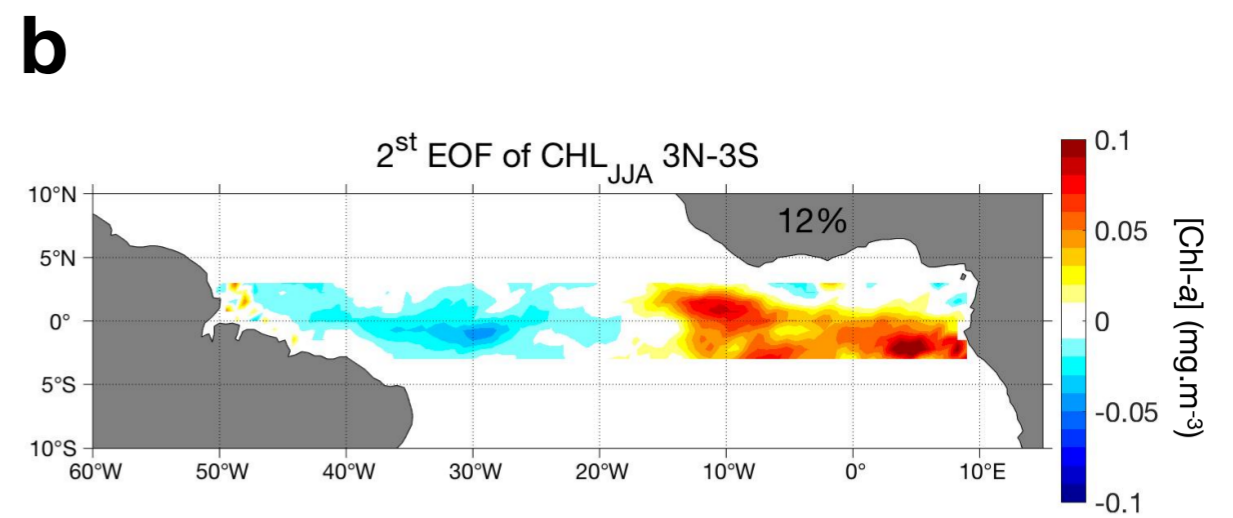
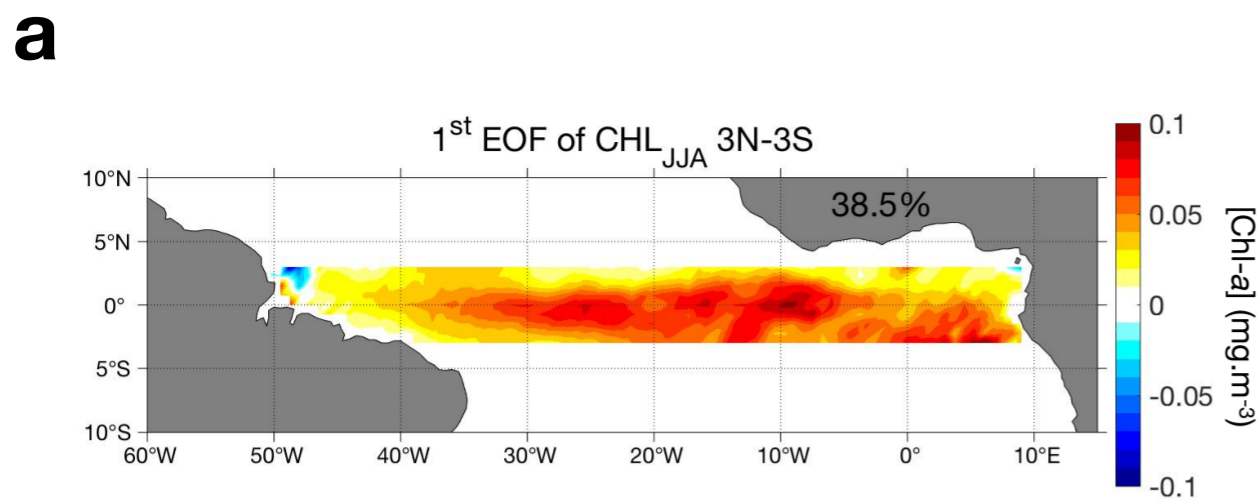


Figure S4: Maps of the two leading Empirical Orthogonal Function (EOF) of boreal summer (JJA) interannual Chl-a variability (mg.m⁻³) in the tropical Atlantic ([3°S-3°N, 60°W-15°E]) over the 1998-2018 period. The percentages indicate the explained variance of each mode. Respective normalized Principal Components (PC1 and PC2) are shown in panel **c** and **d**.